Heliyon 9 (2023) e12667

Contents lists available at ScienceDirect

Heliyon

journal homepage: www.cell.com/heliyon

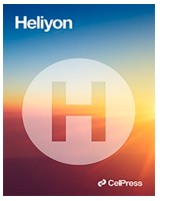

Research article

Insight into free energy and dynamic cross-correlations of residue for binding affinity of antibody and receptor binding domain SARS-CoV-2

Wei Lim Chong [a,b,c], Patchareenart Saparpakorn [a,b], Chak Sangma [a,b], Vannajan Sanghiran Lee [c,**], Supa Hannongbua [a,b,*]

[a] Department of Chemistry, Faculty of Science, Kasetsart University, Bangkok, 10900, Thailand
[b] Center for Advanced Studies in Nanotechnology for Chemical, Food and Agricultural Industries, KU Institute for Advanced Studies, Kasetsart University, Bangkok, 10900, Thailand
[c] Department of Chemistry, Faculty of Science, Universiti Malaya, Kuala Lumber, 50603, Malaysia

ARTICLE INFO

Keywords:
COVID-19
Protein-protein interaction
Receptor binding protein
MM-GBSA
Molecular dynamics simulations
Elastic network model (dynamic cross-correlations)

ABSTRACT

SARS-CoV-2 virus continues to evolve and mutate causing most of the mutated variants resist to many of the therapeutic monoclonal antibodies (mAbs). Despite several mAbs retained neutralizing capability for Omicron BA.1 and BA.2, reduction in neutralization potency was reported. Hence, effort of searching for mAb that is broader in neutralization breadth without losing the neutralizing ability is continued. MW06 was reported with capability in neutralizing most of the variants of concern (VOC) and it binds to the conserved region (left flank) near epitope mAb sotrovimab (S309). In this study, binding affinity of mAb MW06 and its cocktail formulation with MW05 for receptor binding domain (RBD) SARS-CoV-2 virus was investigated under molecular dynamics simulations (MDs). Binding free energies computed by Molecular Mechanics Generalised Born Surface Area (MM-GBSA) algorithm predicted the binding affinity of MW06 for RBD BA.1 (−53 kcal/mol) as strong as RBD wildtype (−58 kcal/mol) while deterioration was observed for RBD BA.2 (−43 kcal/mol). Alike S309 and MW06, simulated cocktail mAb (MW05 and MW06)-RBD interactions suggested the neutralizing capability of the cocktail formulation for RBD BA.1 and BA.2 reduced. Meanwhile, residue pairs that favour the communication between the mAb and RBD have been identified by decomposing the free energy per pairwise residue basis. Apart from understanding the effects of mutation occurred in the RBD region on human angiotensin-converting enzyme 2 (hACE2) binding, impact of heavily mutated RBD on mAb-RBD interactions was investigated in this study as well. In addition to energetic profile obtained from MDs, plotting the dynamics cross-correlation map of the mAb-RBD complex under elastic network model (ENM) was aimed to understand the cross-correlations between residue fluctuations. It allows simple and rapid analysis on the motions or dynamics of the protein residues of mAbs and RBD in complex. Protein residues having correlated motions are normally part of the structural domains of the protein and their respective motions and protein function are related. Motion of mutated RBD residues and mAb residues was less correlated while their respective interactions energy computed to be higher. The combined techniques of MDs and ENM offered simplicity in

Abbreviations: COVID-19, Coronavirus Disease 2019; MM-GBSA, Molecular mechanics with**generalised Born and surface area solvation**.

* Corresponding author.Department of Chemistry, Faculty of Science, Kasetsart University, Bangkok, 10900, Thailand.
** Corresponding author.
E-mail addresses: vannajan@um.edu.my (V.S. Lee), fscisph@ku.ac.th (S. Hannongbua).

https://doi.org/10.1016/j.heliyon.2022.e12667
Received 5 July 2022; Received in revised form 12 November 2022; Accepted 20 December 2022
Available online 3 January 2023

understanding dynamics and energy contribution that explain binding affinity of mAb-RBD complexes.

1. Introduction

Since the pandemic begins in early 2020, severe acute respiratory syndrome coronavirus 2 (SARS-CoV-2) virus mutated and evolved rather quick to series of variants [1] that widely spread around the world and remains as one of the greatest threats to global public health. SARS-CoV-2 has single-strand positive sense RNA genome and is enveloped like other coronaviruses [2]. Of the four structural proteins of SARS-CoV-2, membrane protein and envelope protein are vital for virus assembly process, nucleocapsid protein encapsulates the viral genome, while the spike (S) protein is the key protein mediates viral entry involving receptor binding and membrane fusion [3,4]. Therefore, S protein has been targeted for therapeutic development including antiviral and vaccine [5,6] due to the facts that, it involves in receptor binding and is recognised by neutralizing antibody for antibody-antigen response, particularly the receptor binding domain (RBD) region [7]. Besides, RBD region has been very much explored as it binds to human angiotensin-converting enzyme 2 (hACE2) that is abundantly found in epithelial cells to initiate the viral entry process [8,9]. Heavily mutated RBD might ease the viral entry step as the mutation points harboured by the receptor binding domain (RBM) result a higher binding affinity between RBM and hACE2 to initiate infection [10]. Hence, interfering the communication between RBD and hACE2 would stop the virus from infecting the host cells for replication to cause disease.

Number of cases linked to Omicron variant was on the increasing trend so rapidly and it was being identified as variant of concern (VOC) by the World Health Organisation just two days after the first report was made [11]. Heavily mutated S proteins of Omicron variant has been associated with the possibility of high transmission rate as ample of studies supported that mutations occur on the S protein, particularly the RBD region resulted higher infectivity and immune escape [12-15]. Of the 15 mutations found on the RBD Omicron, 10 are located in the RBM region that hACE2 [16] and some monoclonal antibody (mAbs) bind [17,18]. Some of the mutation points like K417N and N501Y have been well known for their crucial role in enhanced infectivity and responsible for reduction of neutralization capability of mAb [13,19,20]. Successful case of using single mAb and antibody cocktail in treating Ebola disease [21] is not just a key milestone but also become the driven force in developing mAbs for prevention as well as treatment for SARS-CoV-2. Studies and efforts to evaluate neutralizing activity of mAbs for Omicron, especially those candidates that entered clinical trials as therapeutic have been ramped up since Omicron was reported. Some of the antibodies suffered total activity loss while neutralizing activity of some of the Ab weakened or minimally reduced [22]. MAb that failed to neutralize SARS-CoV-2 variants or with diminished efficacy mainly are those targeting the RBM, a region that is heavily mutated. Therefore, mAbs recognize and target the non-RBM region or the most conserved region received increasing attention.

However, studies revealed S309, a mAb that target one of the conserved regions and is currently undergoing clinical trial [23-25] suffered from dampen neutralizing capability for Omicron BA.1 [26-28]. Hence, evaluating binding affinity of mAb MW06 for Omicrons become our interest in this study. MW06 bind to the left flank [29] of the RBD (S309 binds to the right flank) has strong profile of neutralizing activity and cross-reactivity for SARS-CoV-1 and SARS-CoV-2 [30]. Neutralizing capability of MW06 for Omicrons (BA.1 and BA.2) was predicted under molecular dynamics simulations (MDs). Simulated binding interactions and calculated binding free energy of MW06-RBD Omicron series were compared to MW06-RBD of wildtype (WT) SARS-CoV-2. Moreover, decomposing the binding free energy of the mAb-RBD complexes allows identification of residue-residue interactions contributed for binding affinity.

Similarly, complexes containing S309 and RBD of BA.1 and BA.2 were explored under the same approach to understand unfavourable residue-residue interactions that weaken the binding interactions. Apart from single mAbs, binding interactions of cocktail antibody and RBDs were also simulated to estimate the strength of combining mAbs MW06 and MW05 in blocking the RBD-hACE2 interactions, especially for Omicrons. Cocktail antibody MW06 and MW05 was previously reported for disrupting the binding activity between RBD (Alpha, Beta, Gamma and Kappa variants) and hACE2 with strong neutralizing strength ($EC_{50} < 0.02$ μg/ml) [30].

Dynamics and mobility of the RBD residues could pose an impact on the hACE2-RBD binding that contribute to infectivity [31]. A single mutation point would not only alter the local environment alone but also the global motions of the protein [32] what is more when the RBD mutations is massive. Therefore, a closer view on dynamics of proteins would be useful to understand if movement of the amino acid residues found in different regions of the protein is correlated and how they move in relation to each other. Correlations between residue pairs of two interacting proteins could be revealed by residue fluctuations under elastic network model (ENM) without calculating the decomposition energy of interfacial residues located within the binding interface. ENM addresses the shortcomings of MD simulations that consume times and relying on sophisticated architecture of computation. DynOmics [33] is the online ENM server available that integrates gaussian network model and anisotropic network model to compute the dynamics of protein-protein complexes near native state. These allow simple and rapid analysis on the motions or dynamics of the proteins. Dynamics of loop, domain and subunit, and the rotation of side chain are important motions that allow proteins to communicate and result biological functions [34]. Protein residues having correlated motions are normally part of the structural domains of the protein and their respective motions and protein function are related. ENM has demonstrated its strength in correlating the computed protein motion to protein dynamics observed through experimental investigation [35].

In this work, we explored the potential of MW06 and its cocktail antibody to bind with RBD SARS-CoV-2 especially Omicron subvariant BA.1 and BA.2 using a combined technique of MDs and ENM. MDs include the protein flexibility in solution and obtain the binding free energy between each complex while ENM allows fast visualisation to observe the correlation motion of amino acid

residues by generating the DCC map. Combination of MDs and ENM techniques was first employed to understand the how mutations of RBD impacting mAb-RBD binding. The combined techniques of MDs and ENM offered simplicity in correlating dynamics and energy contribution as interacting residues are highly correlated in motions and very often accompanied by a low residue energy. To gain an insight into how mutations impact mAb-RBD binding, we observed the motion of mAb-RBD residues especially the regions that harboured the mutated RBD residues. Mutation that harms the mAb-RBD binding, as suggested by a higher free energy, has less correlated motion with interacting mAb.

2. Methodology

2.1. Modelling of the protein complexes

The template structures described in Table 1 were first examined for missing residues or loop. Gaps between the chains have been closed by adding the missing residues under UCSF Chimera programme, candidate version 1.16 [36], interface to Modeller version 10 [37-39]. Model with the lowest normalized discrete optimized protein energy (zDOPE) score [40] was selected as the initial three-dimensional structure for subsequent steps. Three-dimensional structure of RBD Omicron BA.1 and BA.2 were constructed by mutating the amino acids of RBD WT using UCSF Chimera programme and the top model was selected. For Ab-RBD complexes of Beta and Delta variants, RBD obtained from PDB 7LYN and PDB 7V8B were superimposed to the RBD WT in template structure. Details of Ab-RBD complexes are described in Table 1.

2.2. Molecular dynamics simulations

Protonation states of all the protein complexes were assigned by APBS server (http://server.poissonboltzmann.org/pdb2pqr) [41] at pH 7.0 under AMBER forcefield. The outputs were under tleap module of AMBER20 programme with AMBER forcefield ff19SB [42] loaded to describe the molecular properties of the proteins. Each complex was contained in an octahedral box that solvated with TIP3P water while counterions $Na+$ or Cl^-ions were added for charge neutralization. Non-bonded interactions with cut off of 12 Å and the Particle Mesh Ewald (PME) method were used to compute the electrostatic interactions. Covalent bonds involved hydrogen atoms were constrained by the SHAKE algorithm while temperature along MDs was controlled by the Langevin dynamics. All complexes underwent MDs using a time step of 2 fs

First minimization worked under constant volume, involved a total of 2000 steps, beginning with 1000 steps of steepest descent and followed by another 1000 steps of conjugate gradient. At this stage, all protein residues were fixed using a force constant of 100 kcal/mol $Å^2$. Second minimization worked under the same parameters except the force constant was removed, allowing proteins and water molecules move freely. During the 60 ps long of heating step, the temperature of the simulated systems was increased to 310 K under NVT dynamics while the force constant that hold the protein fixed in position had been reduced to 10 kcal/mol. It was followed by 1 ns long of NPT equilibration that occur at 310 K and constant pressure at 1 atm, before the production run. Trajectories of 200 ns were collected and were processed under CPPTRAJ module [43] for subsequent analysis. The root mean squares deviations (RMSDs) of all Cα-atoms of protein complexes were calculated with using the initial MD structure as reference over 200 ns to account for the structural stability and conformational change during dynamics process. Molecular Mechanics-Generalised Born Solvent Area (MM-GBSA) [44] method was applied for binding free energy and decomposed binding free energy calculations. Altogether, 1000 snapshots were extracted from the last 20 ns of production trajectories for free energy calculations. To map the important residues that are

Table 1
Ab-RBD and hACE2-RBD complexes that were prepared for MDs.

System	Description	Source of structure
RBD-hACE2 (PDB: 6MJ0)	WT	PDB 6MJ0
	Beta	RBD taken from PDB: 7LYN
	Delta	RBD taken from PDB: 7V8B
	Omicron BA.1	Mutated RBD WT
	Omicron BA.2	Mutated RBD WT
MW06-RBD (PDB: 7DPM)	WT	PDB 7DPM
	Beta	RBD taken from PDB 7LYN
	Delta	RBD taken from PDB 7V8B
	Omicron BA.1	Mutated RBD WT
	Omicron BA.2	Mutated RBD WT
S309-RBD (PDB: 7R6W)	WT	PDB 7R6W
	Beta	RBD taken from PDB 7LYN
	Delta	RBD taken from PDB 7V8B
	Omicron BA.1	Mutated RBD WT
	Omicron BA.2	Mutated RBD WT
Cocktail-RBD	WT	Superimpose the MW06-RBD and MW05-RBD complexes to form the cocktail mAb-complexes
	Beta	
(PDB: 7DPM and PDB: 7DK0)	Delta	
	Omicron BA.1	
	Omicron BA.2	

contributing for protein binding, mAb and RBD residues found within 4 Å of binding vicinity were included for pairwise residue interaction energy calculations. Interaction of one residue with all other residues in 4 Å was calculated. Apart from energy calculations, hydrogen bond (H-bond) was also examined to understand the intermolecular interactions of the proteins in depth. Hydrogen bonds with occupancy percentage lower than 30% were excluded for discussion.

3. Results and discussion

3.1. Binding interactions between hACE2 and RBD of SARS-CoV-2 variants

Through MDs, binding strength between the mutated RBD (Delta and Omicrons) and hACE2 was explored. From the binding free energy (Δ_{GB}) obtained from MM-GBSA tabulated in Table S1, affinity of RBD for hACE2 was ranked, RBD Delta (−59.78 kcal/mol) ranked the first, followed by RBD BA.1 (−51.72 kcal/mol), RBD WT (−47.76 kcal/mol), and RBD BA.2 (−46.26 kcal/mol). A study has suggested that binding between RBD Delta and hACE2 was the strongest compared to RBD WT and Omicron [45]. The same study also argued that the binding affinity of RBD WT and Omicron for hACE2 show no noticeable difference. In addition, the heavily mutated Omicron RBD was predicted to have no stronger binding effect with hACE2 under deep mutation scanning [46] as the mutations that enhance the binding of RBD and hACE2 are balanced by the mutations that reduce the binding activity. Here, similar pattern was observed where the difference of binding free energy of WT and BA.1 was <4 kcal/mol and hence their binding affinity for hACE2 was of similar. BA.2 and WT have very close Δ_{GB} was hence predicted to bind with hACE2 not as strong as BA.1. Nevertheless, recent computer aided studies suggested that RBD BA.2 interacted with hACE2 with much lower binding free energy than RBD WT and even RBD BA.1 [47,48]. The difference of binding free energy between Delta and WT was however significant, 12 kcal/mol or 25% lower, achieved good agreement with previous findings. Recent crystal and cryo-EM structures of Omicron in complexed with hACE2 revealed that RBD Omicron and WT bind to hACE2 with equal strength as mutations that facilitate the binding balanced by mutations that are making the binding less favorable [49].

3.2. Ab-RBDs binding to disrupt binding activity of RBD and hACE2

From MDs, binding free energy of MW06-RBD WT and MW06-RBD Beta as computed by MM-GBSA algorithm was −58.15 kcal/mol, and −57.69 kcal/mol, respectively (Table 2). Since MW06 exhibited neutralization potential towards WT, Alpha, Beta, Gamma and Kappa variants [30], its estimated binding free energy of −58.15 kcal/mol was then used as a benchmark to evaluate if MW06 is capable of neutralizing other variants like Delta and Omicrons upon binding with the RBD.

MW06-RBD Delta has binding free energy of −53.71 kcal/mol while MW06-RBD BA.1 has binding free energy of −52.71 kcal/mol, approximately 5 kcal/mol or ∼9% of higher than the benchmark. BA.2 was however observed a much higher binding free energy relative to WT and BA.1, almost 15 kcal/mol higher than WT. From the estimated binding free energy, MW06 is predicted to retain its neutralization effects towards Delta and the two Omicrons upon RBD binding with expectation of reduced efficacy for BA.2 case. S309 that binds to the 'right flank' of the RBD (MW06 binds to the left flank, Fig. 1a) as shown in Fig. 1b, has its binding free energy increased the most for BA.1 and BA.2 compared to other variants, from −54.80 kcal/mol to ∼ −33 kcal/mol, varied almost 39%. S309 has demonstrated its neutralizing effects for WT and the five VOC but efficacy reduced when it comes to BA.1. Thus, higher binding free energy of BA.1 and BA.2 relative to WT correlated to the experimental findings.

3.3. Residue pairs interactions for mAb-RBD binding

Dissecting the protein-protein interactions mediated in the binding vicinity is essential to understand and explain the residue interactions responsible for the binding affinity. Residues that come to interact within 4 Å in the binding vicinity were first identified.

Table 2
Binding free energy of MW06-RBDs and S309-RBDs complexes.

Antibody	Energy Term (kcal/mol)	Complex				
		SARS-CoV-2 (WT)	Beta	Delta	Omicron BA.1	Omicron BA.2
MW06	VDW	−86.81 ± 0.19	−87.84 ± 0.21	−77.85 ± 0.15	−89.38 ± 0.16	−88.33 ± 0.23
	EEL	−86.39 ± 0.55	−61.77 ± 0.72	5.52 ± 0.49	157.27 ± 0.64	127.20 ± 0.89
	EGB	123.08 ± 0.49	100.12 ± 0.64	25.57 ± 0.43	−113.19 ± 0.59	−74.14 ± 0.90
	ESURF	−8.03 ± 0.015	−8.20 ± 0.020	−6.86 ± 0.012	−7.41 ± 0.013	−7.68 ± 0.024
	Δ_{GB}	−58.15 ± 0.18	−57.69 ± 0.20	−53.62 ± 0.19	−52.71 ± 0.17	−42.96 ± 0.21
S309	VDW	−89.00 ± 0.21	−86.59 ± 0.29	−77.67 ± 0.20	−80.47 ± 0.25	−79.88 ± 0.15
	EEL	−185.61 ± 1.02	−24.88 ± 1.08	−31.74 ± 0.58	−78.06 ± 1.40	−62.86 ± 0.98
	EGB	227.98 ± 0.92	80.47 ± 0.97	75.04 ± 0.61	132.83 ± 1.29	117.26 ± 0.92
	ESURF	−8.16 ± 0.017	−10.97 ± 0.040	−7.07 ± 0.017	−7.57 ± 0.025	−7.23 ± 0.012
	Δ_{GB}	−54.80 ± 0.24	−41.97 ± 0.35	−41.43 ± 0.29	−33.27 ± 0.34	−32.70 ± 0.18

Notes: VDW and EEL are van der Waals and electrostatic contribution, respectively, obtained from molecular mechanics. EGB and ESURF represent polar and nonpolar term of GB model while ΔGB is the binding free energy and is accompanied with the standard error mean of the calculation. Entropy is not being taken into calculation.

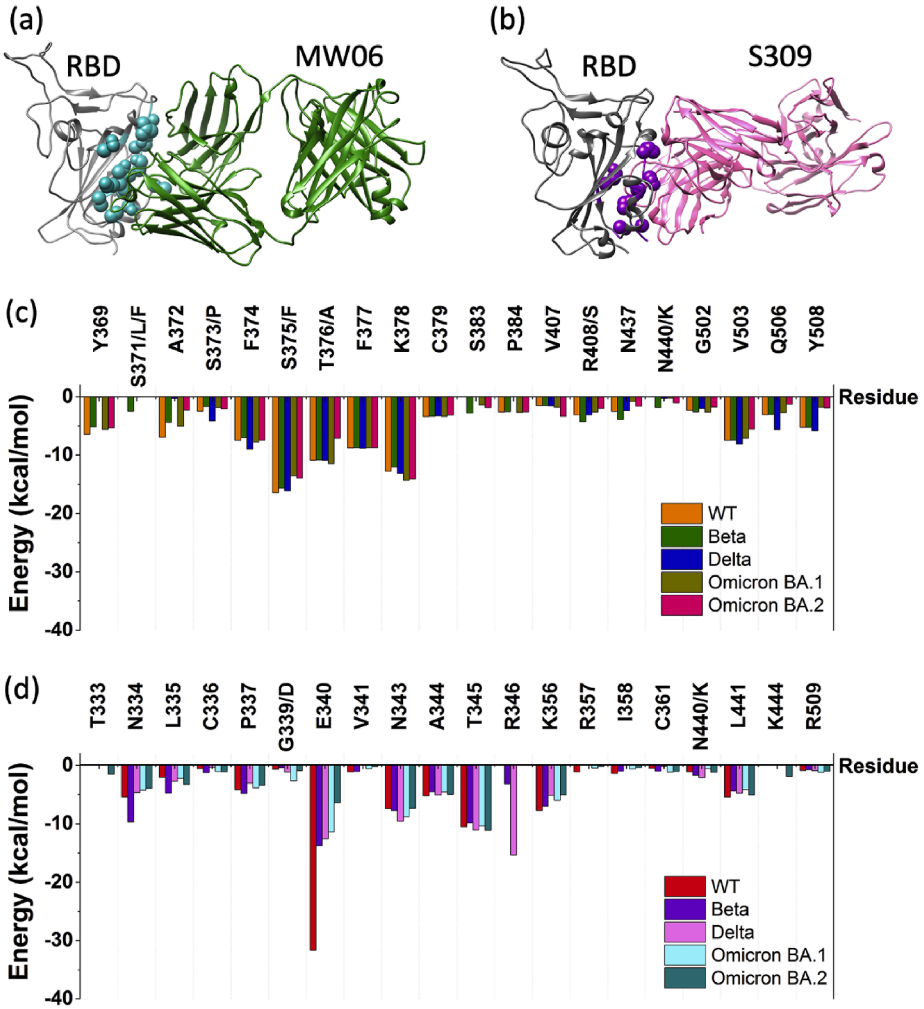

Fig. 1. Binding region of (a) MW06 (left flank) and (b) S309 (right flank) on RBD and the residue pair interactions between RBD and (c) MW06 and (d) S309.

Decomposed binding energy of the residues were calculated in pair-wise basis to locate the important residues (Fig. 1) as well as their residue pair (Table S2 and S3). Altogether, twenty crucial RBD residues were identified. RBD residues, S373P, S375F, and N440K as illustrated in Fig. 1c are the three common mutation points of RBD Omicron lineages, S371L is the unique mutation point of RBD BA.1 while S371F and R408S are specific mutations to BA.2.

From energetic profile, residue 371 of WT and Omicron lineages were not observed to have interactions with MW06. A372 is being sandwiched by two mutation points, S371 L/F and S373P. In MW06-RBD WT complex, A372 communicated with R110 and N322 with energy −4.09 kcal/mol and −1.71 kcal/mol, respectively (Table S2). Absence of the hydrogen bond that formed between R110 and A372 in WT (occupancy 80%) (Table S4), A372-R110 of BA.1 observed a higher energy, −2.29 kcal/mol while A372 of BA.2 was no longer in contact with R110. Nevertheless, interaction of A372 with a polar residue of MW06 remained despite it shifted from N322 to Y107. For BA.1, residue energy changed from −2.51 kcal/mol to −1.85 kcal/mol when proline substituted serine at residue 373. The non-polar P373 shifted its polar residue pair from Y262 to Y107, with energy contribution increased to −0.34 kcal/mol from −1.71 kcal/mol. On the other hand, hydrogen bond of S373-Y262 (occupancy 52%) in WT was not formed between P373-Y107 in BA.1 and BA.2 as the side chain of Y107 and P373 were too far from each other. Replacing the polar serine at position 371 with non-polar leucine or phenylalanine did not cause electrostatic potential varied but S373P mutation in BA.1 and BA.2 resulted the environment around P373 to be more positive charge illustrated in Figure S1a–c.

Substituting serine at residue 375 with phenylalanine caused the residue energy to increase from −16.46 kcal/mol to −13.58 kcal/mol in Omicron BA.1 and −13.96 kcal/mol in Omicron BA.2. Interactions of F375-E111 weakened the most (−1.92 kcal/mol for BA.1; −1.87 kcal/mol for BA.2) compared to S375-E111 (−6.07 kcal/mol) as there is a strong hydrogen bond formed between S375 and E111 with occupancy 88.4%. In addition to S375P mutation, truncating the side chain at residue 376 and replacing the polar threonine by non-polar alanine resulted energy increased to −7.11 kcal/mol from −11 kcal/mol compared to WT and BA.1. Side chain of A376 was too far to communicate with F109 (energy increase >80%) and interaction of A376-Y108 became less favorable compared to

polar-polar interaction of T376-Y108 (energy increase >40%). Figure S1e and S1f described the electrostatic potential surface changed caused by mutation S375F and T376A, respectively. Electrostatic potential surface near Y107 and F109 in BA.1 and BA.2 varied while region near F375 became more negatively charge relative to WT (Figure S1d).

Mutation R408S in RBD BA.2 increased the residue energy from −2.62 kcal/mol to −1.98 kcal/mol, compared to R408 BA.1 due to weakened interactions of S408-Y108 and S408-F109.

Meanwhile the charge of the environment remained unchanged (Figure S1g–i). Strikingly, remarkable residue energy variation occurs on residue Q506 BA.2 and Y508 (Figure S1j–l) for both Omicron lineages although no mutation occurred at these two residues. Q506 of BA.2 observed energy increase more than 50% (from −2.71 to −1.29 kcal/mol) compared to BA.1. Meanwhile, residue energy of Y508 of both BA.1 and BA.2 increased more than 3 kcal/mol relative to WT. Hydrogen bond formed between Y508 RBD WT and E111 of MW06 was not observed in Omicron-MW06 systems owing to the side chain of phenylalanine at position 375 interrupted the side chain interaction between Y508 and E111. As illustrated in Figure S1, the two mutation points did not alter the electrostatic potential much.

Among the 20 RBD residues identified as important for S309-RBD interactions, only two mutated residues unique to BA.1 and BA.2 (G339D and N440K) were interacting with S309 within the binding vicinity [25]. Binding of S309 to RBD Omicron was predicted to be negatively impacted by mutation occurs at residue G339, T345 and R346. However, studies suggested heavily mutated RBD Omicron did not abolish the mAb-RBD binding although S309 suffered increased IC_{50} value [50] and reduced neutralizing activity about 3 folds [26-28]. As shown in Fig. 1d, residue energy of G339 of WT, was rather small (−0.67 kcal/mol) and the energy went lower to −2.62 kcal/mol when aspartic acid substituted glycine at this position in BA.1. In S309-RBD WT complex, D339 residue interacted with two tyrosine residues of S309, Y32 and Y100. Substitution of negatively charged amino acid at residue 339 impacted its adjacent residue E340 as residue energy E340 BA.1 increased from −31.66 kcal/mol to −11.40 kcal/mol, almost 64% higher relative to WT and the energy even went higher in BA.2, −6.39 kcal/mol. Substitution of aspartic acid at residue 339 altered the electrostatic potential in the region and hindered the protein communication between S309 and RBD since D339 and E340 were negatively charged. Residue D339 (Figure S2b and S2c) together with E340 resulted that region to be more negatively charged compared to WT (Figure S2a). Also, E340 of BA.1 and BA.2 was not forming hydrogen bonds with S309 residues (A104, W105, F106 and G107) like WT. In addition, dynamics of the side chain of E340 in BA.1 and BA.2 varied significantly. Side chain E340 BA.1 moved to the S309 site interacting with the polar residues A104, W105, F105 and G107 like WT while E340 BA.2 move away from the interacting site.

N440K could be another concerning mutation point that interfere mAb-RBD interactions as polar amino acid was substituted with a positively charged amino acid. In term of residue energy, N440 of WT has energy of −1.07 kcal/mol and it rises to −0.54 kcal/mol upon N440K mutation in BA.1 but it went lower to −1.13 kcal/mol in BA.2. Although N440K mutation is a common mutation point BA.1 and BA.2 shared, side chain of K440 experienced different dynamics. Side chain of K440 BA.1 moved away from S259 of S309 while it moved closer to interact with S259 BA.2, resulted residue energy low as WT. Substituting asparagine at residue 440 (Figure S2d–S2f) with a positively charged lysine resulted that particular region charged more positive compared to WT.

Hydrogen bond network of the mAb-RBD complexes is described in Table S4. There are 11 hydrogen bonds with occupancy >30% found in MW06-RBD WT complex and the number reduced to 7 for MW06-RBD BA.1 and 6 in MW06-BA.2. In S309-RBD systems, number of hydrogen bonds reduced tremendously from 8 to 2 for BA.1 while BA.2 was able to keep 6 hydrogen bonds with S309. The number of hydrogen bonds reduced largely because of absence of hydrogen bond formed between E340 of RBD Omicrons and the four residues of S309, A104,W105, F106 and G107.

3.4. Binding of cocktail antibody of MW05 and MW06 and RBDs

Cocktail of MW05 and MW06 has a binding free energy of −91.49 kcal/mol and −104.51 kcal/mol (Table 3) in complexed with RBD WT and RBD Beta, respectively. Meanwhile, the binding free energy of cocktail-Delta reported as −112.76 kcal/mol, −80.64 kcal/mol for the BA.1 and −93.08 kcal/mol for BA.2. Cocktail of MW05 and MW06 that is binding with RBD WT and Beta for inhibition [30] has binding free energy in the range of −91 to −104.5 kcal/mol.

Hence, cocktail is predicted to be a potent antiviral mAb for RBD of other SARS-CoV-2 variant if the cocktail-RBD complex has binding free energy within the range or lower than −104 kcal/mol. Despite lacking of lab data to support the neutralizing capability of the cocktail for RBD Delta, however the strong binding strength of cocktail for RBD Delta is suggested by its lower binding free energy.

Table 3
Binding free energy of cocktail antibody-RBDs variants complexes.

Energy Term (kcal/mol)	Complex				
	SARS-CoV-2 (WT)	Beta	Delta	Omicron BA.1	Omicron BA.2
VDW	−185.87 ± 0.27	−172.84 ± 0.29	−187.73 ± 0.52	−179.96 ± 0.38	−210.43 ± 0.44
EEL	−127.04 ± 1.08	−65.74 ± 1.06	26.95 ± 1.13	244.20 ± 1.48	292.35 ± 1.33
EGB	225.36 ± 0.93	162.29 ± 0.98	64.93 ± 1.23	−128.13 ± 1.47	−156.96 ± 1.27
ESURF	−16.96 ± 0.023	−15.19 ± 0.026	−16.91 ± 0.045	−16.76 ± 0.040	−18.04 ± 0.036
Δ_{GB}	−104.51 ± 0.31	−91.49 ± 0.32	−112.76 ± 0.40	−80.64 ± 0.34	−93.08 ± 0.45

Notes: VDW and EEL are van der Waals and electrostatic contribution, respectively, obtained from molecular mechanics. EGB and ESURF represent polar and nonpolar term of GB model while ΔGB is the binding free energy and is accompanied with the standard error mean of the calculations. Entropy is not being taken into calculations.

About 24 kcal/mol higher in binding free energy observed in cocktail mAb-RBD BA.1 complex reflected the neutralization effect of cocktail mAb deteriorated. Nevertheless, binding free energy of BA.2 in complexed with the cocktail mAb was within the range. Several studies demonstrated BA.1 escaped from the neutralization effects of cocktail antibody Regeneron 10933/Regeneron 10987 and LY-CoV016/LY-CoV555 while activity of AZD7442 (combination of AZD8895 and AZD1061) reduced [22,51]. Regeneron cocktail is sensitive to mutation occurred at residue E484, Q493, N440 and G446 while LY-CoV016/LY-CoV555 are sensitive to E484, Q493, N501, and Y505 mutations. For AZD7442 it makes contact with S477, Q493 and G446, hence mutation of these residues harboured by Omicron variant was linked to the reduced antibody activity. Similar to the two single mAbs discussed earlier, cocktail of MW05 and MW06 is predicted to have its neutralizing capability reduced when it comes to Omicron and sub-lineages.

To have a better understanding how mutation points that are unique to BA.1 and BA.2 affected the cocktail mAb-RBD binding, important residues interacted in the binding vicinity within 4 Å were identified. First, the energy profile of the epitope residues of RBD that MW06 bind in the cocktail complex (Fig. 2a) and MW06-RBD (Fig. 2b) were carefully examined. Overall, the residue energy profile of the two systems as described by Fig. 2 was similar. Remarkable difference spotted for residue Y369, A372, S373P and K378. In presence of MW05 in the cocktail complex, residue energy of Y369 and P373 RBD BA.1 and BA.2 went lower while A372 and K378 BA.2 observed to have residue energy increased, in comparison to MW06-RBD complex. From the energy profile of cocktail mAb-RBDs, residue energy of Y369 BA.1 and BA.2 was 4.85 kcal/mol and 3.93 kcal/mol lower than WT whereas P373 BA.1 and BA.2 was 2.98 kcal/mol and 6.72 kcal/mol lower than WT. K378 BA.2 higher in energy than K378 WT and BA.1 for about 4 kcal/mol.

Compared to RBD WT, MW05 less interacted with amino acid at position 484, 485, 486, 489, 490, 493, and 494. Among the residues listed, two are the mutated residues, E484A and Q493R. Many mAbs failed or lacked inhibitory activity against Omicrons due to these two mutated residues. Details of the interactions involved the two mutated residues and the interacting MW05 residues are described in Figure S3. Residue energy increased from −30 kcal/mol to −3.4 kcal/mol when alanine (Figure S3c) substituted glutamic acid (Figure S3a) at residue 484 in BA.1. In addition, strong electrostatic interactions between E484 and R260 MW05 was absent in Omicron sub-variants. The non-polar A484 residue interfaced with polar side chain of Y317 and was too far from the non-polar residue,

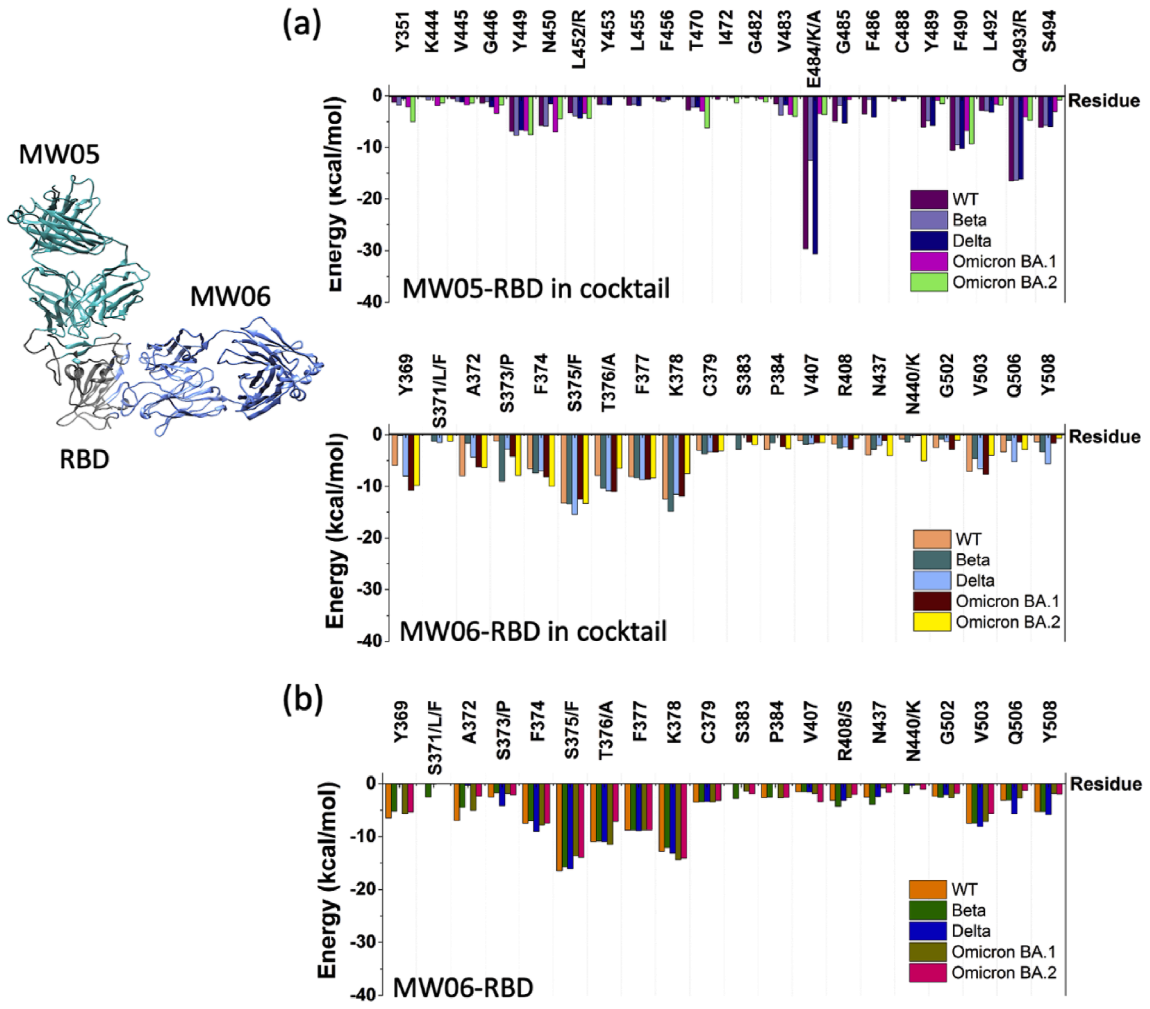

Fig. 2. Pairwise residue energy between interactions of RBDs and (a) cocktail antibody MW05/MW06 and (b) MW06 in complex.

W94. Arginine at position 493 (Figure S3d) did not interact with the glycine at residue 312, 313, and 314 like its WT, Q493 (Figure S3b). In addition, Y317 MW05 was no longer interacting with R493 but L311. Failure to make contact with the few serine amino acids and Y317 resulted the residue energy of Q493R increased 76%, from −16.5 kcal/mol to −4.04 kcal/mol. Here, we observed mutation E484A and Q493R enabled sub-variants of Omicron to escape from being neutralised by MW05. Effects of RBD residues of BA.1 and BA.2 that interacted with the cocktail mAb with higher residue energy were balanced by the residues that observed a much lower energy, resulted overall binding free energy of BA.2 lower than the BA.1.

3.5. Fluctuation and dynamic cross-correlation of the protein residues

RMSF of hACE2-RBDs, MW06-RBDs, S309-RBDs and cocktail of MW05/MW06-RBDs were described in Figure S4 to understand how mutations altered the flexibility of the individual protein residues in complex. In general, RMSF is computed to study the dynamics of protein residues after mutations [52-55]. There are more flexible residues in complex containing RBD Omicron. Mutations of the RBD Omicron were not only increasing the flexibility of some residues but also causing certain regions of the RBD to be more rigid and it is consistent with a previous report that study effect of mutations on RBD flexibility [56].

On the other hand, protein residues having correlated motions are normally part of the structural domains of the protein and their respective motions and protein function are related [57]. DCC map is commonly employed to study the correlations of the motions of different parts of two interacting molecules [57,58]. In addition, obtaining a DCC map through ENM is much simpler and direct. To cross-correlate the motions of the protein residues for hACE2-RBD WT and mAb-RBDs complexes, DCC maps were plotted using the final snapshot sampled from the production run of MDs. In Fig. 3, correlation of the motions of the residues in the hACE2-RBD WT complex was portrayed through the DCC map.

Region 1 and 2 correspond to hACE2 residues 19–106, 321–331 and 349–356 and the entire RBD (residue 333–526), while region 3 harboured hACE2 residues 389–392 and RBD residues 473–488. Although the whole RBD has correlated motion with hACE2, motion of certain RBD regions including the RBM appeared to have a much higher correlation as showed in orange and green parts of the RBD in Fig. 3. In addition, the motions of hACE2 residues in region 3 as coloured in purple correlated with the RBD residues in region 1. Through the cross-correlations analysis, mutations occur in RBD and the effect in hACE2-RBD binding can be correlated. HACE2-RBD binding is impacted even if the mutation points of RBD are located very far away from the RBM since the motions of the whole RBD and hACE2 were correlated. Even a single mutation point would alter the global motions of the protein [32] what is more when the RBD mutations is massive. Hence, the cross-correlations of motions between the hACE2 and RBD could further clarify how mutations on RBD changing the intermolecular interactions between hACE2 and RBD upon binding. Also, the rationale of different epitope sites of RBD to be targeted by mAbs to establish neutralization is justified where mAb binding site on RBD is not limited to the RBM but other sites as reported [29].

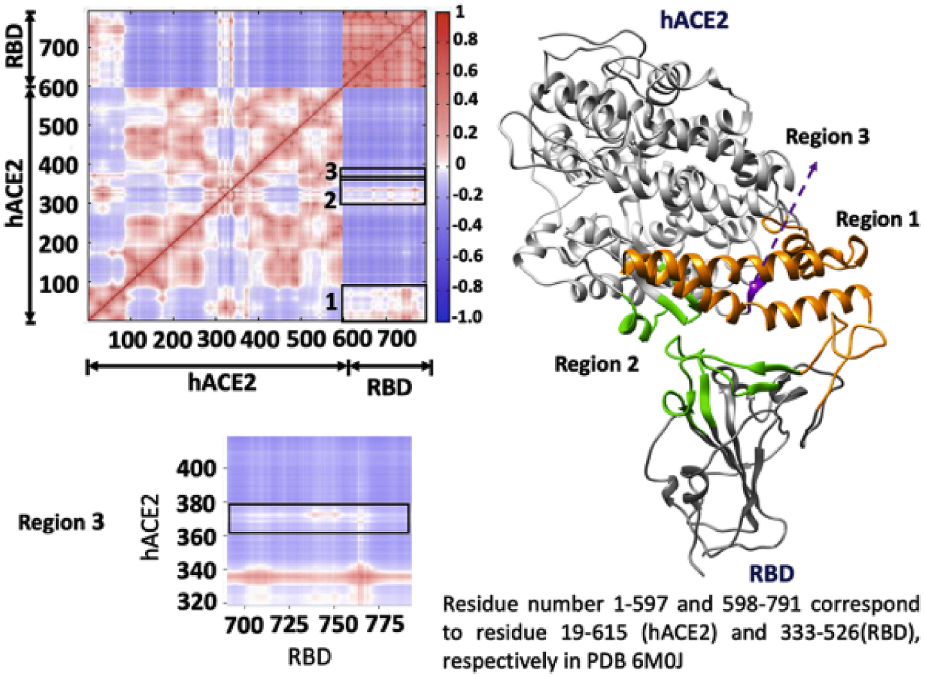

Fig. 3. Dynamic cross-correlation map of hACE2-RBD WT. Regions coloured in red indicated the motions between the residue pairs are correlated. Representation of hACE2-RBD WT generated using final snapshot of the complex from MDs. Region 3 in the dynamic cross-correlation map has been enlarged. Location of the highlighted regions in map were shown in the structure of hACE2-RBD WT and was coloured in orange, green, and purple. (For interpretation of the references to colour in this figure legend, the reader is referred to the Web version of this article.)

DCC map was also plotted to correlate the motions of MW06 (Fig. 4) and S309 (Fig. 5) upon association with RBDs. The DCC maps of MW06 in complexed with RBD WT (Fig. 4a), Omicron BA.1 (Fig. 4b) and Omicron BA.2 (Fig. 4c) are almost identical expect the intensity that represent degree of correlation between the motions of the two proteins. Region 1 of MW06 interfaced with RBD region accommodating mutation points S371 L/F, S373P, S375F and T376A (residue 483–488 in DCC map Fig. 4b and c) observed to have less correlation in motions. Meanwhile, in region 2, MW06 interacting with part of the RBM region that harbour mutation points Q493R, Q498R, N501Y and Y505H. Mutation points in regions 1 have demonstrated their role in increasing the residue energy (Table S2) but not the mutations points in region 2 as illustrated in Fig. 1. Nevertheless, neighbouring residue of mutation points in region 2, Q506 and Y508 interacting with MW06 with higher residue energy. Apart from the increasing residue energy, motions of mAb-RBD residues in these two regions for Omicron systems were less correlated as well.

DCC map of S309 and RBDs captured a slight different dynamic profile compared to MW06-RBD complexes as plotted in Fig. 5. Although two distinct regions were observed like the MW06-RBD systems (Fig. 5a), region 1 of S309-RBDs has a lower degree of correlation in motions. S309 residues G103-L110 in region 1 have corelated motions with the whole RBD and appeared to be a distinctive bar, however the correlation become less as indicated by the reduced intensity in S309-RBD Omicron BA.1 (Fig. 5b) and BA.2 (Fig. 5c) systems. These residues are interacting with E340 with higher energy (Table S3). As discussed earlier, effect of G339D mutation was not observed on residue 339 but its adjacent amino acid residue E340. Overall, heavily mutated RBD of Omicrons has altered the dynamics of the S309-RBD complex resulting the motions of the protein residues less correlated.

Despite plotting DCC map under ENM method is simple and direct, it relies on the availability of three-dimensional structure. When the three-dimensional model of a particular complex is absent, modelling approach is required, like the mAb-RBD complexes there were modelled in this study. In addition, the modelled complexes need to undergo MDs for refinements or corrections under protein forcefield prior to extraction of the dynamics or motion of the protein residues.

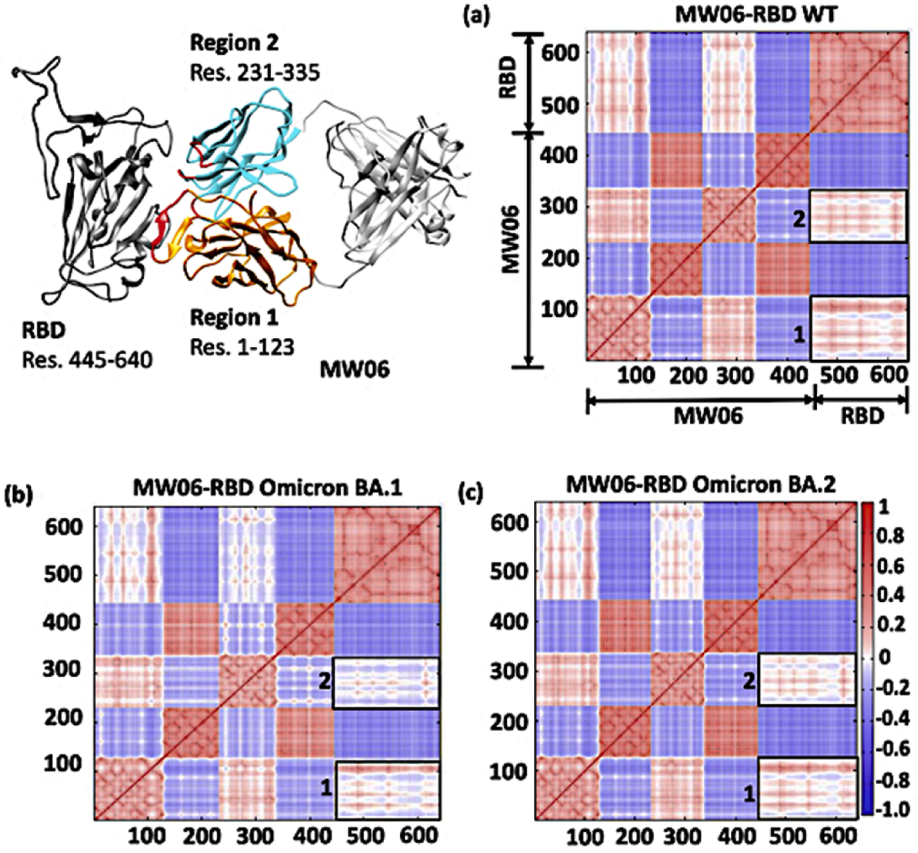

Fig. 4. Dynamic cross-correlation map of MW06 in complexed with (a) RBD WT, (b) RBD Omicron BA.1 and (c) RBD Omicron BA.2. Structure of MW06-RBD WT was generated using the final snapshot obtained from MDs. Part of the antibody in region 1 and 2 were coloured in orange and cyan blue, respectively, with the most intense part coloured in red. Refer to PDB 7DPM, residue number 1–444 corresponded to heavy chain (1–230) and light chain (1–214) of MW06 while 445–640 belong to RBD residues (333–528). (For interpretation of the references to colour in this figure legend, the reader is referred to the Web version of this article.)

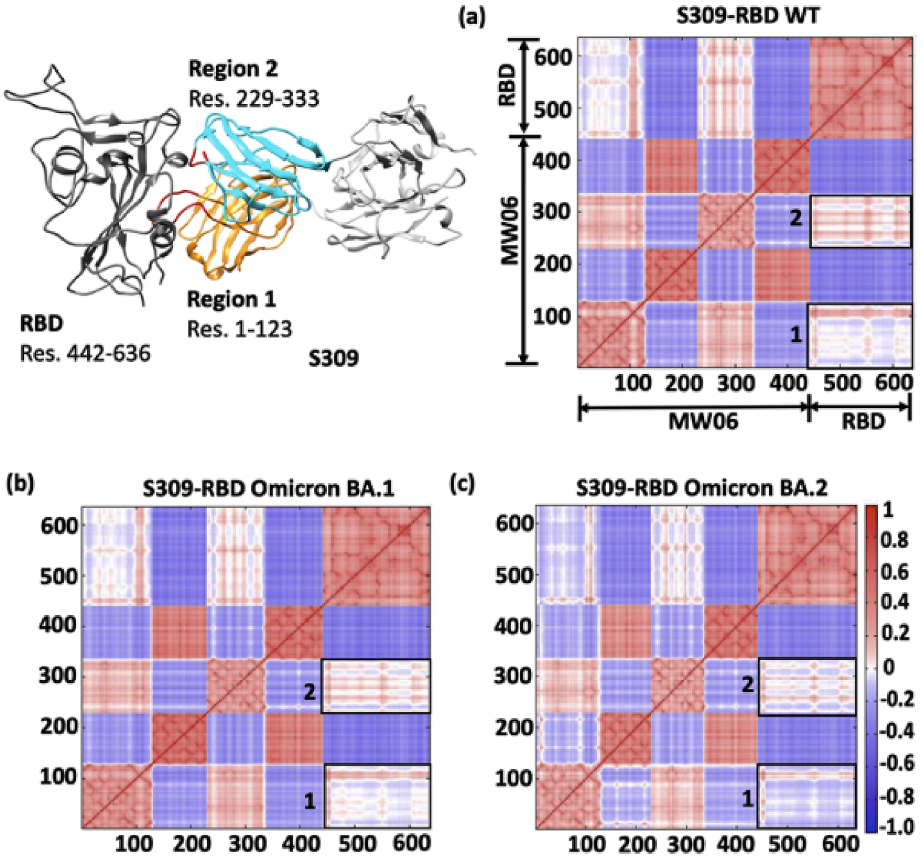

Fig. 5. Dynamic cross-correlation map of S309 in complexed with (a) RBD WT, (b) RBD Omicron BA.1 and (c) RBD Omicron BA.2. Structure of S309-RBD WT was generated using the final snapshot obtained from MDs. Part of the antibody in region 1 and 2 were coloured in orange and cyan blue, respectively, with the most intense part coloured in red. Refer to PDB 7R6W, residue number 1–441 corresponded to heavy chain (1–228) and light chain (1–213) of S309 while 442–636 belong to RBD residues (333–527). (For interpretation of the references to colour in this figure legend, the reader is referred to the Web version of this article.)

4. Conclusion

MDs and ENM were coupled to evaluate the binding affinity of mAb MW06 and RBD SARS-CoV-2 especially Omicron subvariant, BA.1 and BA.2 and understand how mutations weaken the mAb-RBD interactions that impact the neutralizing activity. We first investigated the binding affinity of mAb MW06 for RBD BA.1 and BA.2 and extended to the cocktail mAb that consists of MW06 and MW05. Binding strength of MW06 for RBD WT > Beta > Delta > BA.2 BA.1 was predicted. From energetic profile, binding strength of MW06 for BA.1 was predicted to be comparable with WT in the range of < - 50 kcal/mol but efficacy was however expected to reduce for BA.2 (−43 kcal/mol). Cocktail of MW05 and MW06 demonstrated its high potential to bind with RBD Delta (−113 kcal/mol) as its binding free energy is 8 kcal/mol lowered than the WT. Nevertheless, the binding strength of cocktail mAbs towards RBD Omicron subvariants was not as strong as the WT and Delta as the free energy went higher. Cocktail mAbs approach was not found to be more effective than single mAb and in fact suffered from weakening binding affinity for BA.1 and BA.2. The observation is in line with S309-RBD complexes where S309 has its neutralizing strength reduced for BA.1 and BA.2. In addition, it implies that not all the cocktail approaches are effective and the choice of using a single mAb could be more suitable than a cocktail, like the failure of employing cocktail antibody containing three mAbs for treating Ebola [59] was reported. From DCC map plotted under ENM, dynamics of the mAb-RBD complexes were captured to understand correlations of the motions of protein residues. RBD WT regions in hACE2-RBD WT complex that were correlated in motions with hACE2 revealed possible binding sites for mAbs binding. Also, upon association of RBD and mAbs, dynamics of the RBD changed. MAb MW06 residues that are interacting with RBD region harbouring mutation like S371L, S373P, S375F and T376A have their motion less correlated and higher in residue energy. Therefore, effects of mutation in weakening mAb-RBD interactions were illustrated by higher residue energy together with less motion correlation. Combining findings obtained from MDs and dynamics computed by ENM, effects of each individual mutation point and their adjacent residues in mAb-RBD binding can be easily studied through free energy calculations and fluctuations of protein residues that give rise to DCC map. Taken together the computed free energy and the correlation of motion illustrated by DCC maps, fast and rapid observation in binding affinity of mAb and RBD is possible.

Acknowledgement

This work was financially supported by the Office of the Ministry of Higher Education, Science, Research and Innovation; and the Thailand Science Research and Innovation through the Kasetsart University Reinventing University Program 2021 and Kasetsart University Research and Development Institute (FF(KU)11.64). Chong Wei Lim is grateful to Kasetsart University for a Postdoctoral fellowship. The Universiti Malaya is acknowledged for generous supporting on computing time and facilities.

Appendix A. Supplementary data

Supplementary data related to this article can be found at https://doi.org/10.1016/j.heliyon.2022.e12667.

References

[1] J.A. Plante, B.M. Mitchell, K.S. Plante, K. Debbink, S.C. Weaver, V.D. Menachery, The variant gambit: COVID-19's next move, Cell Host Microbe 29 (2021) 508–515, https://doi.org/10.1016/j.chom.2021.02.020.

[2] R. Lu, X. Zhao, J. Li, P. Niu, B. Yang, H. Wu, W. Wang, H. Song, B. Huang, N. Zhu, Y. Bi, X. Ma, F. Zhan, L. Wang, T. Hu, H. Zhou, Z. Hu, W. Zhou, L. Zhao, J. Chen, Y. Meng, J. Wang, Y. Lin, J. Yuan, Z. Xie, J. Ma, W.J. Liu, D. Wang, W. Xu, E.C. Holmes, G.F. Gao, G. Wu, W. Chen, W. Shi, W. Tan, Genomic characterisation and epidemiology of 2019 novel coronavirus: implications for virus origins and receptor binding, Lancet (London, England) 395 (2020) 565–574, https://doi.org/10.1016/S0140-6736(20)30251-8.

[3] S. Belouzard, J.K. Millet, B.N. Licitra, G.R. Whittaker, Mechanisms of coronavirus cell entry mediated by the viral spike protein, Viruses 4 (2012) 1011–1033, https://doi.org/10.3390/v4061011.

[4] T. Tang, M. Bidon, J.A. Jaimes, G.R. Whittaker, S. Daniel, Coronavirus membrane fusion mechanism offers a potential target for antiviral development, Antivir. Res. 178 (2020), 104792, https://doi.org/10.1016/j.antiviral.2020.104792.

[5] L. Du, Y. He, Y. Zhou, S. Liu, B.-J. Zheng, S. Jiang, The spike protein of SARS-CoV–a target for vaccine and therapeutic development, Nat. Rev. Microbiol. 7 (2009) 226–236, https://doi.org/10.1038/nrmicro2090.

[6] L. Du, Y. Yang, Y. Zhou, L. Lu, F. Li, S. Jiang, MERS-CoV spike protein: a key target for antivirals, Expert Opin. Ther. Targets 21 (2017) 131–143, https://doi.org/10.1080/14728222.2017.1271415.

[7] L. Premkumar, B. Segovia-Chumbez, R. Jadi, D.R. Martinez, R. Raut, A.J. Markmann, C. Cornaby, L. Bartelt, S. Weiss, Y. Park, C.E. Edwards, E. Weimer, E. M. Scherer, N. Rouphael, S. Edupuganti, D. Weiskopf, L.V. Tse, Y.J. Hou, D. Margolis, A. Sette, M.H. Collins, J. Schmitz, R.S. Baric, A.M. de Silva, The receptor-binding domain of the viral spike protein is an immunodominant and highly specific target of antibodies in SARS-CoV-2 patients, Sci. Immunol. 5 (2020), https://doi.org/10.1126/sciimmunol.abc8413 eabc8413.

[8] M. Hoffmann, H. Kleine-Weber, S. Schroeder, N. Krüger, T. Herrler, S. Erichsen, T.S. Schiergens, G. Herrler, N.-H. Wu, A. Nitsche, M.A. Müller, C. Drosten, S. Pöhlmann, SARS-CoV-2 cell entry depends on ACE2 and TMPRSS2 and is blocked by a Clinically Proven Protease Inhibitor, Cell 181 (2020) 271–280, https://doi.org/10.1016/j.cell.2020.02.052, e8.

[9] A.C. Walls, Y.-J. Park, M.A. Tortorici, A. Wall, A.T. McGuire, D. Veesler, Structure, Function, and antigenicity of the SARS-CoV-2 spike glycoprotein, Cell 181 (2020) 281–292, https://doi.org/10.1016/j.cell.2020.02.058, e6.

[10] J. Chen, R. Wang, M. Wang, G.-W. Wei, Mutations strengthened SARS-CoV-2 infectivity, J. Mol. Biol. 432 (2020) 5212–5226, https://doi.org/10.1016/j.jmb.2020.07.009.

[11] R. Viana, S. Moyo, D.G. Amoako, H. Tegally, C. Scheepers, C.L. Althaus, U.J. Anyaneji, P.A. Bester, M.F. Boni, M. Chand, W.T. Choga, R. Colquhoun, M. Davids, K. Deforche, D. Doolabh, L. du Plessis, S. Engelbrecht, J. Everatt, J. Giandhari, M. Giovanetti, D. Hardie, V. Hill, N.-Y. Hsiao, A. Iranzadeh, A. Ismail, C. Joseph, R. Joseph, L. Koopile, S.L. Kosakovsky Pond, M.U.G. Kraemer, L. Kuate-Lere, O. Laguda-Akingba, O. Lesetedi-Mafoko, R.J. Lessells, S. Lockman, A.G. Lucaci, A. Maharaj, B. Mahlangu, T. Maponga, K. Mahlakwane, Z. Makatini, G. Marais, D. Maruapula, K. Masupu, M. Matshaba, S. Mayaphi, N. Mbhele, M.B. Mbulawa, A. Mendes, K. Mlisana, A. Mnguni, T. Mohale, M. Moir, K. Moruisi, M. Mosepele, G. Motsatsi, M.S. Motswaledi, T. Mphoyakgosi, N. Msomi, P.N. Mwangi, Y. Naidoo, N. Ntuli, M. Nyaga, L. Olubayo, S. Pillay, B. Radibe, Y. Ramphal, U. Ramphal, J.E. San, L. Scott, R. Shapiro, L. Singh, P. Smith-Lawrence, W. Stevens, A. Strydom, K. Subramoney, N. Tebeila, D. Tshiabuila, J. Tsui, S. van Wyk, S. Weaver, C.K. Wibmer, E. Wilkinson, N. Wolter, A.E. Zarebski, B. Zuze, D. Goedhals, W. Preiser, F. Treurnicht, M. Venter, C. Williamson, O.G. Pybus, J. Bhiman, A. Glass, D.P. Martin, A. Rambaut, S. Gaseitsiwe, A. von Gottberg, T. de Oliveira, Rapid epidemic expansion of the SARS-CoV-2 Omicron variant in southern Africa, Nature 603 (2022) 679–686, https://doi.org/10.1038/s41586-022-04411-y.

[12] M.I. Barton, S.A. MacGowan, M.A. Kutuzov, O. Dushek, G.J. Barton, P.A. van der Merwe, Effects of common mutations in the SARS-CoV-2 Spike RBD and its ligand, the human ACE2 receptor on binding affinity and kinetics, Elife 10 (2021), https://doi.org/10.7554/eLife.70658.

[13] Q. Li, J. Nie, J. Wu, L. Zhang, R. Ding, H. Wang, Y. Zhang, T. Li, S. Liu, M. Zhang, C. Zhao, H. Liu, L. Nie, H. Qin, M. Wang, Q. Lu, X. Li, J. Liu, H. Liang, Y. Shi, Y. Shen, L. Xie, L. Zhang, X. Qu, W. Xu, W. Huang, Y. Wang, SARS-CoV-2 501Y.V2 variants lack higher infectivity but do have immune escape, Cell 184 (2021) 2362–2371, https://doi.org/10.1016/j.cell.2021.02.042, e9.

[14] H.M. Mengist, A.J. Kombe Kombe, D. Mekonnen, A. Abebaw, M. Getachew, T. Jin, Mutations of SARS-CoV-2 spike protein: implications on immune evasion and vaccine-induced immunity, Semin. Immunol. 55 (2021), 101533, https://doi.org/10.1016/j.smim.2021.101533.

[15] F. Lou, M. Li, Z. Pang, L. Jiang, L. Guan, L. Tian, J. Hu, J. Fan, H. Fan, Understanding the secret of SARS-CoV-2 variants of concern/interest and immune escape, Front. Immunol. 12 (2021), https://doi.org/10.3389/fimmu.2021.744242.

[16] J. Lan, J. Ge, J. Yu, S. Shan, H. Zhou, S. Fan, Q. Zhang, X. Shi, Q. Wang, L. Zhang, X. Wang, Structure of the SARS-CoV-2 spike receptor-binding domain bound to the ACE2 receptor, Nature 581 (2020) 215–220, https://doi.org/10.1038/s41586-020-2180-5.

[17] S.J. Zost, P. Gilchuk, J.B. Case, E. Binshtein, R.E. Chen, J.P. Nkolola, A. Schäfer, J.X. Reidy, A. Trivette, R.S. Nargi, R.E. Sutton, N. Suryadevara, D.R. Martinez, L. E. Williamson, E.C. Chen, T. Jones, S. Day, L. Myers, A.O. Hassan, N.M. Kafai, E.S. Winkler, J.M. Fox, S. Shrihari, B.K. Mueller, J. Meiler, A. Chandrashekar, N. B. Mercado, J.J. Steinhardt, K. Ren, Y.-M. Loo, N.L. Kallewaard, B.T. McCune, S.P. Keeler, M.J. Holtzman, D.H. Barouch, L.E. Gralinski, R.S. Baric, L.B. Thackray, M.S. Diamond, R.H. Carnahan, J.E. Crowe, Potently neutralizing and protective human antibodies against SARS-CoV-2, Nature 584 (2020) 443–449, https://doi.org/10.1038/s41586-020-2548-6.

[18] L. Liu, P. Wang, M.S. Nair, J. Yu, M. Rapp, Q. Wang, Y. Luo, J.F.-W. Chan, V. Sahi, A. Figueroa, X.V. Guo, G. Cerutti, J. Bimela, J. Gorman, T. Zhou, Z. Chen, K.-Y. Yuen, P.D. Kwong, J.G. Sodroski, M.T. Yin, Z. Sheng, Y. Huang, L. Shapiro, D.D. Ho, Potent neutralizing antibodies against multiple epitopes on SARS-CoV-2 spike, Nature 584 (2020) 450–456, https://doi.org/10.1038/s41586-020-2571-7.

[19] W.T. Harvey, A.M. Carabelli, B. Jackson, R.K. Gupta, E.C. Thomson, E.M. Harrison, C. Ludden, R. Reeve, A. Rambaut, S.J. Peacock, D.L. Robertson, C.-19 G.U.K. (COG-U), Consortium, SARS-CoV-2 variants, spike mutations and immune escape, Nat. Rev. Microbiol. 19 (2021) 409–424, https://doi.org/10.1038/s41579-021-00573-0.

[20] Y. Cao, A. Yisimayi, Y. Bai, W. Huang, X. Li, Z. Zhang, T. Yuan, R. An, J. Wang, T. Xiao, S. Du, W. Ma, L. Song, Y. Li, X. Li, W. Song, J. Wu, S. Liu, X. Li, Y. Zhang, B. Su, X. Guo, Y. Wei, C. Gao, N. Zhang, Y. Zhang, Y. Dou, X. Xu, R. Shi, B. Lu, R. Jin, Y. Ma, C. Qin, Y. Wang, Y. Feng, J. Xiao, X.S. Xie, Humoral immune response to circulating SARS-CoV-2 variants elicited by inactivated and RBD-subunit vaccines, Cell Res. 31 (2021) 732–741, https://doi.org/10.1038/s41422-021-00514-9.

[21] D. Corti, L.A. Purcell, G. Snell, D. Veesler, Tackling COVID-19 with neutralizing monoclonal antibodies, Cell 184 (2021) 3086–3108, https://doi.org/10.1016/j.cell.2021.05.005.

[22] L.A. VanBlargan, J.M. Errico, P.J. Halfmann, S.J. Zost, J.E. Crowe, L.A. Purcell, Y. Kawaoka, D. Corti, D.H. Fremont, M.S. Diamond, An infectious SARS-CoV-2 B.1.1.529 Omicron virus escapes neutralization by therapeutic monoclonal antibodies, Nat. Med. (2022), https://doi.org/10.1038/s41591-021-01678-y.

[23] A. Gupta, Y. Gonzalez-Rojas, E. Juarez, M. Crespo Casal, J. Moya, D.R. Falci, E. Sarkis, J. Solis, H. Zheng, N. Scott, A.L. Cathcart, C.M. Hebner, J. Sager, E. Mogalian, C. Tipple, A. Peppercorn, E. Alexander, P.S. Pang, A. Free, C. Brinson, M. Aldinger, A.E. Shapiro, Early treatment for Covid-19 with SARS-CoV-2 neutralizing antibody Sotrovimab, N. Engl. J. Med. 385 (2021) 1941–1950, https://doi.org/10.1056/NEJMoa2107934.

[24] A.L. Cathcart, C. Havenar-Daughton, F.A. Lempp, D. Ma, M.A. Schmid, M.L. Agostini, B. Guarino, J. Di iulio, L.E. Rosen, H. Tucker, J. Dillen, S. Subramanian, B. Sloan, S. Bianchi, D. Pinto, C. Saliba, K. Culap, J.A. Wojcechowskyj, J. Noack, J. Zhou, H. Kaiser, A. Chase, M. Montiel-Ruiz, E. Dellota, A. Park, R. Spreafico, A. Sahakyan, E.J. Lauron, N. Czudnochowski, E. Cameroni, S. Ledoux, A. Werts, C. Colas, L. Soriaga, A. Telenti, L.A. Purcell, S. Hwang, G. Snell, H.W. Virgin, D. Corti, C.M. Hebner, The dual function monoclonal antibodies VIR-7831 and VIR-7832 demonstrate potent in vitro and in vivo activity against SARS-CoV-2, BioRxiv, https://doi.org/10.1101/2021.03.09.434607, 2021.

[25] D. Pinto, Y.-J. Park, M. Beltramello, A.C. Walls, M.A. Tortorici, S. Bianchi, S. Jaconi, K. Culap, F. Zatta, A. De Marco, A. Peter, B. Guarino, R. Spreafico, E. Cameroni, J.B. Case, R.E. Chen, C. Havenar-Daughton, G. Snell, A. Telenti, H.W. Virgin, A. Lanzavecchia, M.S. Diamond, K. Fink, D. Veesler, D. Corti, Cross-neutralization of SARS-CoV-2 by a human monoclonal SARS-CoV antibody, Nature 583 (2020) 290–295, https://doi.org/10.1038/s41586-020-2349-y.

[26] E. Cameroni, J.E. Bowen, L.E. Rosen, C. Saliba, S.K. Zepeda, K. Culap, D. Pinto, L.A. VanBlargan, A. De Marco, J. di Iulio, F. Zatta, H. Kaiser, J. Noack, N. Farhat, N. Czudnochowski, C. Havenar-Daughton, K.R. Sprouse, J.R. Dillen, A.E. Powell, A. Chen, C. Maher, L. Yin, D. Sun, L. Soriaga, J. Bassi, C. Silacci-Fregni, C. Gustafsson, N.M. Franko, J. Logue, N.T. Iqbal, I. Mazzitelli, J. Geffner, R. Grifantini, H. Chu, A. Gori, A. Riva, O. Giannini, A. Ceschi, P. Ferrari, P.E. Cippà, A. Franzetti-Pellanda, C. Garzoni, P.J. Halfmann, Y. Kawaoka, C. Hebner, L.A. Purcell, L. Piccoli, M.S. Pizzuto, A.C. Walls, M.S. Diamond, A. Telenti, H. W. Virgin, A. Lanzavecchia, G. Snell, D. Veesler, D. Corti, Broadly neutralizing antibodies overcome SARS-CoV-2 Omicron antigenic shift, Nature 602 (2022) 664–670, https://doi.org/10.1038/s41586-021-04386-2.

[27] D. Planas, N. Saunders, P. Maes, F. Guivel-Benhassine, C. Planchais, J. Buchrieser, W.-H. Bolland, F. Porrot, I. Staropoli, F. Lemoine, H. Péré, D. Veyer, J. Puech, J. Rodary, G. Baele, S. Dellicour, J. Raymenants, S. Gorissen, C. Geenen, B. Vanmechelen, T. Wawina-Bokalanga, J. Martí-Carreras, L. Cuypers, A. Sève, L. Hocqueloux, T. Prazuck, F.A. Rey, E. Simon-Loriere, T. Bruel, H. Mouquet, E. André, O. Schwartz, Considerable escape of SARS-CoV-2 Omicron to antibody neutralization, Nature 602 (2022) 671–675, https://doi.org/10.1038/s41586-021-04389-z.

[28] L. Liu, S. Iketani, Y. Guo, J.F.-W. Chan, M. Wang, L. Liu, Y. Luo, H. Chu, Y. Huang, M.S. Nair, J. Yu, K.K.-H. Chik, T.T.-T. Yuen, C. Yoon, K.K.-W. To, H. Chen, M. T. Yin, M.E. Sobieszczyk, Y. Huang, H.H. Wang, Z. Sheng, K.-Y. Yuen, D.D. Ho, Striking antibody evasion manifested by the Omicron variant of SARS-CoV-2, Nature 602 (2022) 676–681, https://doi.org/10.1038/s41586-021-04388-0.

[29] W. Dejnirattisai, D. Zhou, H.M. Ginn, H.M.E. Duyvesteyn, P. Supasa, J.B. Case, Y. Zhao, T.S. Walter, A.J. Mentzer, C. Liu, B. Wang, G.C. Paesen, J. Slon-Campos, C. López-Camacho, N.M. Kafai, A.L. Bailey, R.E. Chen, B. Ying, C. Thompson, J. Bolton, A. Fyfe, S. Gupta, T.K. Tan, J. Gilbert-Jaramillo, W. James, M. Knight, M. W. Carroll, D. Skelly, C. Dold, Y. Peng, R. Levin, T. Dong, A.J. Pollard, J.C. Knight, P. Klenerman, N. Temperton, D.R. Hall, M.A. Williams, N.G. Paterson, F.K. R. Bertram, C.A. Siebert, D.K. Clare, A. Howe, J. Radecke, Y. Song, A.R. Townsend, K.-Y.A. Huang, E.E. Fry, J. Mongkolsapaya, M.S. Diamond, J. Ren, D.I. Stuart, G.R. Screaton, The antigenic anatomy of SARS-CoV-2 receptor binding domain, Cell 184 (2021) 2183–2200, https://doi.org/10.1016/j.cell.2021.02.032, e22.

[30] W. Jiang, J. Wang, S. Jiao, C. Gu, W. Xu, B. Chen, R. Wang, H. Chen, Y. Xie, A. Wang, G. Li, D. Zeng, J. Zhang, M. Zhang, S. Wang, M. Wang, X. Gui, Characterization of MW06, a human monoclonal antibody with cross-neutralization activity against both SARS-CoV-2 and SARS-CoV, mAbs 13 (2021), 1953683, https://doi.org/10.1080/19420862.2021.1953683.

[31] A. Spinello, A. Saltalamacchia, A. Magistrato, Is the rigidity of SARS-CoV-2 spike receptor-binding Motif the Hallmark for its enhanced infectivity? Insights from all-atom simulations, J. Phys. Chem. Lett. 11 (2020) 4785–4790, https://doi.org/10.1021/acs.jpclett.0c01148.

[32] W.L. Chong, V. Vao-soongnern, P. Nimmanpipug, C. Tayapiwatana, J.-H. Lin, Y.-L. Lin, H.Y. Chee, S.M. Zain, N.A. Rahman, V.S. Lee, Molecular dynamics simulations and Gaussian network model for designing antibody mimicking protein towards dengue envelope protein, J. Mol. Liq. 346 (2022), 118086, https://doi.org/10.1016/j.molliq.2021.118086.

[33] H. Li, Y.-Y. Chang, J.Y. Lee, I. Bahar, L.-W. Yang, DynOmics: dynamics of structural proteome and beyond, Nucleic Acids Res. 45 (2017) W374–W380, https://doi.org/10.1093/nar/gkx385.

[34] T. Haliloglu, I. Bahar, Adaptability of protein structures to enable functional interactions and evolutionary implications, Curr. Opin. Struct. Biol. 35 (2015) 17–23, https://doi.org/10.1016/j.sbi.2015.07.007.

[35] Y. Wang, A.J. Rader, I. Bahar, R.L. Jernigan, Global ribosome motions revealed with elastic network model, J. Struct. Biol. 147 (2004) 302–314, https://doi.org/10.1016/j.jsb.2004.01.005.

[36] E.F. Pettersen, T.D. Goddard, C.C. Huang, G.S. Couch, D.M. Greenblatt, E.C. Meng, T.E. Ferrin, UCSF Chimera-a visualization system for exploratory research and analysis, J. Comput. Chem. 25 (2004) 1605–1612, https://doi.org/10.1002/jcc.20084.

[37] A. Fiser, R.K. Do, A. Sali, Modeling of loops in protein structures, Protein Sci. 9 (2000) 1753–1773, https://doi.org/10.1110/ps.9.9.1753.

[38] A. Sali, T.L. Blundell, Comparative protein modelling by satisfaction of spatial restraints, J. Mol. Biol. 234 (1993) 779–815, https://doi.org/10.1006/jmbi.1993.1626.

[39] A. Fiser, A. Sali, Modeller: generation and refinement of homology-based protein structure models, Methods Enzymol. 374 (2003) 461–491, https://doi.org/10.1016/S0076-6879(03)74020-8.

[40] M.-Y. Shen, A. Sali, Statistical potential for assessment and prediction of protein structures, Protein Sci. 15 (2006) 2507–2524, https://doi.org/10.1110/ps.062416606.

[41] E. Jurrus, D. Engel, K. Star, K. Monson, J. Brandi, L.E. Felberg, D.H. Brookes, L. Wilson, J. Chen, K. Liles, M. Chun, P. Li, D.W. Gohara, T. Dolinsky, R. Konecny, D.R. Koes, J.E. Nielsen, T. Head-Gordon, W. Geng, R. Krasny, G.-W. Wei, M.J. Holst, J.A. McCammon, N.A. Baker, Improvements to the APBS biomolecular solvation software suite, Protein Sci. 27 (2018) 112–128, https://doi.org/10.1002/pro.3280.

[42] C. Tian, K. Kasavajhala, K.A.A. Belfon, L. Raguette, H. Huang, A.N. Migues, J. Bickel, Y. Wang, J. Pincay, Q. Wu, C. Simmerling, ff19SB: amino-acid-specific protein backbone parameters trained against quantum mechanics energy surfaces in solution, J. Chem. Theor. Comput. 16 (2020) 528–552, https://doi.org/10.1021/acs.jctc.9b00591.

[43] D.R. Roe, T.E. Cheatham III, PTRAJ and CPPTRAJ: software for processing and analysis of molecular dynamics trajectory data, J. Chem. Theor. Comput. 9 (2013) 3084–3095, https://doi.org/10.1021/ct400341p.

[44] A. Onufriev, D. Bashford, D.A. Case, Exploring protein native states and large-scale conformational changes with a modified generalized Born model, Proteins Struct. Funct. Genet. 55 (2004) 383–394, https://doi.org/10.1002/prot.20033.

[45] L. Wu, L. Zhou, M. Mo, T. Liu, C. Wu, C. Gong, K. Lu, L. Gong, W. Zhu, Z. Xu, SARS-CoV-2 Omicron RBD shows weaker binding affinity than the currently dominant Delta variant to human ACE2, Signal Transduct. Targeted Ther. 7 (2022) 8, https://doi.org/10.1038/s41392-021-00863-2.

[46] T.N. Starr, A.J. Greaney, S.K. Hilton, D. Ellis, K.H.D. Crawford, A.S. Dingens, M.J. Navarro, J.E. Bowen, M.A. Tortorici, A.C. Walls, N.P. King, D. Veesler, J. D. Bloom, Deep mutational scanning of SARS-CoV-2 Receptor binding domain reveals constraints on folding and ACE2 binding, Cell 182 (2020) 1295–1310, https://doi.org/10.1016/j.cell.2020.08.012, e20.

[47] M. Golcuk, A. Yildiz, M. Gur, Omicron BA.1 and BA.2 variants increase the interactions of SARS-CoV-2 Spike glycoprotein with ACE2, BioRxiv, https://doi.org/10.1101/2021.12.06.471377, 2022.

[48] J. Chen, G.-W. Wei, Omicron BA.2 (B.1.1.529.2): high potential for becoming the next dominant variant, J. Phys. Chem. Lett. (2022) 3840–3849, https://doi.org/10.1021/acs.jpclett.2c00469.

[49] P. Han, L. Li, S. Liu, Q. Wang, D. Zhang, Z. Xu, P. Han, X. Li, Q. Peng, C. Su, B. Huang, D. Li, R. Zhang, M. Tian, L. Fu, Y. Gao, X. Zhao, K. Liu, J. Qi, G.F. Gao, P. Wang, Receptor binding and complex structures of human ACE2 to spike RBD from Omicron and Delta SARS-CoV-2, Cell (2022), https://doi.org/10.1016/j.cell.2022.01.001.

[50] Y. Cao, J. Wang, F. Jian, T. Xiao, W. Song, A. Yisimayi, W. Huang, Q. Li, P. Wang, R. An, J. Wang, Y. Wang, X. Niu, S. Yang, H. Liang, H. Sun, T. Li, Y. Yu, Q. Cui, S. Liu, X. Yang, S. Du, Z. Zhang, X. Hao, F. Shao, R. Jin, X. Wang, J. Xiao, Y. Wang, X.S. Xie, Omicron escapes the majority of existing SARS-CoV-2 neutralizing antibodies, Nature (2021), https://doi.org/10.1038/s41586-021-04385-3.

[51] W. Dejnirattisai, J. Huo, D. Zhou, J. Zahradník, P. Supasa, C. Liu, H.M.E. Duyvesteyn, H.M. Ginn, A.J. Mentzer, A. Tuekprakhon, R. Nutalai, B. Wang, A. Dijokaite, S. Khan, O. Avinoam, M. Bahar, D. Skelly, S. Adele, S.A. Johnson, A. Amini, T.G. Ritter, C. Mason, C. Dold, D. Pan, S. Assadi, A. Bellass, N. Omo-Dare, D. Koeckerling, A. Flaxman, D. Jenkin, P.K. Aley, M. Voysey, S.A. Costa Clemens, F.G. Naveca, V. Nascimento, F. Nascimento, C. Fernandes da Costa, P. C. Resende, A. Pauvolid-Correa, M.M. Siqueira, V. Baillie, N. Serafin, G. Kwatra, K. Da Silva, S.A. Madhi, M.C. Nunes, T. Malik, P.J.M. Openshaw, J.K. Baillie, M. G. Semple, A.R. Townsend, K.-Y.A. Huang, T.K. Tan, M.W. Carroll, P. Klenerman, E. Barnes, S.J. Dunachie, B. Constantinides, H. Webster, D. Crook, A.J. Pollard, T. Lambe, C. Conlon, A.S. Deeks, J. Frater, L. Frending, S. Gardiner, A. Jämsén, K. Jeffery, T. Malone, E. Phillips, L. Rothwell, L. Stafford, J.K. Baillie, M. G. Semple, P.J.M. Openshaw, G. Carson, B. Alex, P. Andrikopoulos, B. Bach, W.S. Barclay, D. Bogaert, M. Chand, K. Chechi, G.S. Cooke, A. da Silva Filipe, T. de Silva, A.B. Docherty, G. dos Santos Correia, M.-E. Dumas, J. Dunning, T. Fletcher, C.A. Green, W. Greenhalf, J.L. Griffin, R.K. Gupta, E.M. Harrison, J.A. Hiscox, A.Y. Wai Ho, P.W. Horby, S. Ijaz, S. Khoo, P. Klenerman, A. Law, M.R. Lewis, S. Liggi, W.S. Lim, L. Maslen, A.J. Mentzer, L. Merson, A.M. Meynert, S.C. Moore, M. Noursadeghi, M. Olanipekun, A. Osagie, M. Palmarini, C. Palmieri, W.A. Paxton, G. Pollakis, N. Price, A. Rambaut, D.L. Robertson, C.D. Russell, V. Sancho-Shimizu, C.J. Sands, J.T. Scott, L. Sigfrid, T. Solomon, S. Sriskandan, D. Stuart, C. Summers, O.V. Swann, Z. Takats, P. Takis, R.S. Tedder, A.A.R. Thompson, E. C. Thomson, R.S. Thwaites, L.C.W. Turtle, M. Zambon, H. Hardwick, C. Donohue, F. Griffiths, W. Oosthuyzen, C. Donegan, R.G. Spencer, L. Norman, R. Pius, T. M. Drake, C.J. Fairfield, S.R. Knight, K.A. Mclean, D. Murphy, C.A. Shaw, J. Dalton, M. Girvan, E. Saviciute, S. Roberts, J. Harrison, L. Marsh, M. Connor, S. Halpin, C. Jackson, C. Gamble, D. Plotkin, J. Lee, G. Leeming, A. Law, M. Wham, S. Clohisey, R. Hendry, J. Scott-Brown, V. Shaw, S.E. McDonald, S. Keating, K.A. Ahmed, J.A. Armstrong, M. Ashworth, I.G. Asiimwe, S. Bakshi, S.L. Barlow, L. Booth, B. Brennan, K. Bullock, B.W.A. Catterall, J.J. Clark, E.A. Clarke, S. Cole, L. Cooper, H. Cox, C. Davis, O. Dincarslan, C. Dunn, P. Dyer, A. Elliott, A. Evans, L. Finch, L.W.S. Fisher, T. Foster, I. Garcia-Dorival, P. Gunning, C. Hartley, R.L. Jensen, C.B. Jones, T.R. Jones, S. Khandaker, K. King, R.T. Kiy, C. Koukorava, A. Lake, S. Lant, D. Latawiec, L. Lavelle-Langham, D. Lefteri, L. Lett, L.A. Livoti, M. Mancini, S. McDonald, L. McEvoy, J. McLauchlan, S. Metelmann, N.S. Miah, J. Middleton, J. Mitchell, S.C. Moore, E.G. Murphy, R. Penrice-Randal, J. Pilgrim, T. Prince, W. Reynolds, P.M. Ridley, D. Sales, V.E. Shaw, R.K. Shears, B. Small, K.S. Subramaniam, A. Szemiel, A. Taggart, J. Tanianis-Hughes, J. Thomas, E. Trochu, L. van Tonder, E. Wilcock, J.E. Zhang, L. Flaherty, N. Maziere, E. Cass, A.D. Carracedo, N. Carlucci, A. Holmes, H. Massey, L. Murphy, S. McCafferty, R. Clark, A. Fawkes, K. Morrice, A. Maclean, N. Wrobel, L. Donnelly, A. Coutts, K. Hafezi, L. MacGillivray, T. Gilchrist, K. Adeniji, D. Agranoff, K. Agwuh, D. Ail, E.L. Aldera, A. Alegria, S. Allen, B. Angus, A. Ashish, D. Atkinson, S. Bari, G. Barlow, S. Barnass, N. Barrett, C. Bassford, S. Basude, D. Baxter, M. Beadsworth, J. Bernatoniene, J. Berridge, C. Berry, N. Best, P. Bothma, D. Chadwick, R. Brittain-Long, N. Bulteel, T. Burden, A. Burtenshaw, V. Caruth, D. Chadwick, D. Chambler, N. Chee, J. Child, S. Chukkambotla, T. Clark, P. Collini, C. Cosgrove, J. Cupitt, M.-T. Cutino-Moguel, P. Dark, C. Dawson, S. Dervisevic, P. Donnison, S. Douthwaite, A. Drummond, I. DuRand, A. Dushianthan, T. Dyer, C. Evans, C. Eziefula, C. Fegan, A. Finn, D. Fullerton, S. Garg, S. Garg, A. Garg, E. Gkrania-Klotsas, J. Godden, A. Goldsmith, C. Graham, E. Hardy, S. Hartshorn, D. Harvey, P. Havalda, D.B. Hawcutt, M. Hobrok, L. Hodgson, A. Hormis, M. Jacobs, S. Jain, P. Jennings, A. Kaliappan, V. Kasipandian, S. Kegg, M. Kelsey, J. Kendall, C. Kerrison, I. Kerslake, O. Koch, G. Koduri, G. Koshy, S. Laha, S. Laird, S. Larkin, T. Leiner, P. Lillie, J. Limb, V. Linnett, J. Little, M. Lyttle, M. MacMahon, E. MacNaughton, R. Mankregod, H. Masson, E. Matovu, K. McCullough, R. McEwen, M. Meda, G. Mills, J. Minton, M. Mirfenderesky, K. Mohandas, Q. Mok, J. Moon, E. Moore, P. Morgan, C. Morris, K. Mortimore, S. Moses, M. Mpenge, R. Mulla, M. Murphy, M. Nagel, T. Nagarajan, M. Nelson, L. Norris, M.K. O'Shea, I. Otahal, M. Ostermann, M. Pais, C. Palmieri, S. Panchatsharam, D. Papakonstantinou, H. Paraiso, B. Patel, N. Pattison, J. Pepperell, M. Peters, M. Phull, S. Pintus, J.S. Pooni, T. Planche, F. Post, D. Price, R. Prout, N. Rae, H. Reschreiter, T. Reynolds, N. Richardson, M. Roberts, D. Roberts, A. Rose, G. Rousseau, B. Ruge, B. Ryan, T. Saluja, M. L. Schmid, A. Shah, P. Shanmuga, A. Sharma, A. Shawcross, J. Sizer, M. Shankar-Hari, R. Smith, C. Snelson, N. Spittle, N. Staines, T. Stambach, R. Stewart, P. Subudhi, T. Szakmany, K. Tatham, J. Thomas, C. Thompson, R. Thompson, A. Tridente, D. Tupper-Carey, M. Twagira, N. Vallotton, R. Vancheeswaran, L. Vincent-Smith, S. Visuvanathan, A. Vuylsteke, S. Waddy, R. Wake, A. Walden, I. Welters, T. Whitehouse, P. Whittaker, A. Whittington, P. Papineni, M. Wijesinghe, M. Williams, L. Wilson, S. Cole, S. Winchester, M. Wiselka, A. Wolverson, D.G. Wootton, A. Workman, B. Yates, P. Young, N.G. Paterson, M. A. Williams, D.R. Hall, E.E. Fry, J. Mongkolsapaya, J. Ren, G. Schreiber, D.I. Stuart, G.R. Screaton, SARS-CoV-2 Omicron-B.1.1.529 leads to widespread escape from neutralizing antibody responses, Cell (2022), https://doi.org/10.1016/j.cell.2021.12.046.

[52] I. Aier, P.K. Varadwaj, U. Raj, Structural insights into conformational stability of both wild-type and mutant EZH2 receptor, Sci. Rep. 6 (2016), 34984, https://doi.org/10.1038/srep34984.

[53] C.G.P. Doss, B. Rajith, N. Garwasis, P.R. Mathew, A.S. Raju, K. Apoorva, D. William, N.R. Sadhana, T. Himani, I.P. Dike, Screening of mutations affecting protein stability and dynamics of FGFR1—a simulation analysis, Appl. Transl. Genomics. 1 (2012) 37–43, https://doi.org/10.1016/j.atg.2012.06.002.

[54] M.T. Khan, A. Khan, A.U. Rehman, Y. Wang, K. Akhtar, S.I. Malik, D.-Q. Wei, Structural and free energy landscape of novel mutations in ribosomal protein S1 (rpsA) associated with pyrazinamide resistance, Sci. Rep. 9 (2019) 7482, https://doi.org/10.1038/s41598-019-44013-9.

[55] C.V. Kumar, R.G. Swetha, A. Anbarasu, S. Ramaiah, Computational analysis reveals the association of Threonine 118 Methionine mutation in PMP22 resulting in CMT-1A, Adv. Bioinf. 2014 (2014), 502618, https://doi.org/10.1155/2014/502618.

[56] A.L. Alaofi, M. Shahid, Mutations of SARS-CoV-2 RBD may alter its molecular structure to improve its infection efficiency, Biomolecules 11 (2021) 1273, https://doi.org/10.3390/biom11091273.

[57] S.K. Mishra, R.L. Jernigan, Protein dynamic communities from elastic network models align closely to the communities defined by molecular dynamics, PLoS One 13 (2018), e0199225, https://doi.org/10.1371/journal.pone.0199225.

[58] M. Tekpinar, B. Neron, M. Delarue, Extracting dynamical correlations and identifying key residues for allosteric communication in proteins by correlationplus, J. Chem. Inf. Model. 61 (2021) 4832–4838, https://doi.org/10.1021/acs.jcim.1c00742.

[59] S. Mulangu, L.E. Dodd, R.T. Davey, O. Tshiani Mbaya, M. Proschan, D. Mukadi, M. Lusakibanza Manzo, D. Nzolo, A. Tshomba Oloma, A. Ibanda, R. Ali, S. Coulibaly, A.C. Levine, R. Grais, J. Diaz, H.C. Lane, J.-J. Muyembe-Tamfum, The PALM writing group, A randomized, controlled trial of Ebola virus disease therapeutics, N. Engl. J. Med. 381 (2019) 2293–2303, https://doi.org/10.1056/NEJMoa1910993.